2D Inverse Heat Transfer Measurements by IR Thermography in Hypersonic Flows

by F. Avallone*, C. S. Greco** and D. Ekelschot***

*Dept. of Aerospace Engineering, University of Naples, Via Claudio 21, 80125 Napoli, Italy, *francesco.avallone2@unina.it*
**Dept. of Aerospace Engineering, University of Naples, Via Claudio 21, 80125 Napoli, Italy, *carlo.greco@studenti.unina.it*
****Delft University of Technology, Kluyverweg 1, 2629HS Delft, The Netherlands, *D.Ekelschot@student.TUDelft.NL*

Abstract

The purpose of this work is to develop a data reduction technique for the measurement of heat fluxes in hypersonic flows. When dealing with inverse heat transfer problems in which temperature gradients in the solid are high enough (e.g. in case of temperature distributions due Görtler vortices that can have high spatial frequency), tangential conduction is not negligible. The heat flux is estimated by solving a 2-D inverse heat transfer problem. The heat flux distribution is represented by discrete Fourier series, to reduce the computational cost.The data reduction technique has been numerically validated and then applied to experimental tests performed in an hypersonic wind tunnel at Mach number equal to 7.5 on a compression ramp where the instability is generated using a comb-like strip. The heat flux obtained solving the 2-D inverse heat transfer problem is compared with the one obtained solving the 1-D problem to evaluate the effect of the tangential conduction. Results show that the convective heat flux coefficient distribution obtained by the 2-D solution is higher than the one obtained from the 1-D case and that, using the two dimensional approach, a higher resolution of the result is obtained.

NOMENCLATURE

K	thermal conductivity	[W m^{-1} K^{-1}]
ρ	Density	[Kg m^{-3}]
c_p	specific heat	[J Kg^{-1} K^{-1}]
T_{wi}	initial temperature	[K]
q_w	heat flux	[W m^{-1}]
h	convective heat flux coefficient	[W m^{-2} K^{-1}]
T_w	wall temperature	[K]
T_{aw}	adiabatic wall temperature	[K]
T_S	boundary temperature	[K]
Σ	Stefan-Boltzmann constant	[W m^{-2} K^{-4}]
E	surface emissivity of the model	
T_r	reference temperature	[K]
$T_{w_{TH}}$	measured temperature	[K]
$T_{w_{NUM}}$	temperature in inverse problem	[K]
f_s	frequency of acquisition	[Hz]
t_p	test time	[s]
x,y,z	reference system	
T	Time	[s]
N	Number of pixels in spanwise direction	

1 Introduction

In several branches of science and engineering it is important to estimate convective heat flux, e.g., to investigate the higher heat loads encountered in the reattachment region [1] or to study the boundary layer evolution through the use of the Reynolds similarity parameters [2]. Measurement of the convective heat flux is traditionally performed using heat flux sensors such as heated thin-foil, thin film sensors, wall calorimeter and thin-skin sensors [3]. In some cases these sensors cannot be used: temperature distribution is measured directly by means of thermocouples, resistance temperature detectors (RTDs) or infrared (IR) thermography and the surface heat flux distribution is then obtained by solving an inverse heat transfer problem (IHTP) [4]. These problems, usually, are ill-posed since small errors in temperature measurements can cause large errors in the computed heat transfer [5].

Measuring temperature with standard techniques, such as thermocouples or RTDs, each transducer yields the temperature at a single point and the transducer is regarded as being zero-dimensional. In these cases the heat flux is obtained by solving a one dimensional (1-D) IHTP. For the solution of 1-D IHTPs the first approach was proposed by Cook and Felderman [6] who integrated numerically the heat equation and they obtained a relation between heat flux and temperature evolution. Afterwards, many different techniques were proposed by several authors using various mathematical approaches. For example, Ji et al. [7] suggested a method based on the recursive least-squares algorithm for estimating the acting time dependent heat flux while Scarpa and Milano [8] reconstructed the time-dependent surface heat flux by using the Kalman smoothing technique, given the initial temperature distribution and the time-temperature history at an interior location. Raynaud and Beck [9] made a comparison between several methods and proposed to use a space marching scheme. Raynaud and Bransier [10] took into account that material characteristic could be temperature dependant and consequently, the heat equation is a non-linear equation that was solved by a space marching finite difference algorithm using interior temperature measurements at future times. With the aim to reduce the model dimension Shenefelt et al. [11] applied a unit heat flux pulse to a linear conduction model to determine the temperature response and used it to solve the physical problem assembling a Toeplitz matrix on which the singular value decomposition (SVD) was performed.

If the heat flux and consequently also the temperature field exhibit spatial variations, the heat flux evaluation using zero-dimensional sensors can be troublesome [12]. Instead, IR thermography can be very useful; IR camera consists of a two dimensional transducer, allowing for accurate measurements of surface temperature maps even in the presence of relatively high spatial gradients. When compared to standard techniques the use of IR camera, as a temperature transducer in heat transfer measurements, appears advantageous from several points of view [13]: non-intrusive, high sensitivity (up to 20 mK), low response time (down to 20 μs) and it permits an easier evaluation of errors due to tangential conduction.

Using temperature maps obtained by IR camera the heat flux can be estimated solving multidimensional (two dimensional, 2-D, or three dimensional, 3-D) IHTPs. As for the 1-D case also for the multidimensional IHTPs many methods have been presented in literature. The 2-D steady state IHTP was solved by AL-Najemi et al. [14] in a rectangular region using two approaches: least squares coupled with the integral transform method (ITM) and SVD coupled with boundary element method (BEM) considering also the effect of random errors on the accuracy of the prediction. The transient 2-D heat conduction problem was solved, in case that the functional form of the heat transfer coefficient was unknown a priori, by Chen and Wu [15] using an hybrid scheme in which they combined Laplace transform, finite difference discretization and least squares minimization. If the problem requires to estimate two separate heat flux inputs on two boundaries of the model a possible approach was proposed by Tuan et al. [16] who used the Kalman's filter. In the solution of this class of problem also the lagging and damping effects due to the diffusion process must be taken into account, according to Beck [17], using a sequential method. Yang [18] proposed a method in which, in contrast to the traditional approach, the iteration can be done only once and the inverse problem can be solved in the linear domain. For the solution of multidimensional IHTPs Petit et al. [19] and Schrijer and Modenini [20] used the adjoint equation approach coupled to the conjugate gradient method while Huang and Chen [21] used BEM coupled with the conjugate gradient method to solve multidimensional steady state IHTP with arbitrary geometry.

All these IHTPs involve temperature measurements and a mathematical representation of the heat equation. The solution of the heat equation is usually made discretizing the domain by a finite element approach particularly in the two dimensional cases [18,22,23] or by finite difference approach [15].

In the solution of multidimensional IHTPs the number of parameters to determine may increase and consequently the computational cost could be relevant. Several methods are illustrated in literature to reduce the number of parameters to estimate: Videcoq and Petit [24] proposed to solve a reduced model that is built considering only the dominant eigenmodes of the starting matrix and they showed that the approach could be interesting in the three dimensional case where it is possible to solve a system of order 9 instead of a system of order 1331; Park et al. [25] suggested a method based on the Karhunen-Loève Galerkin method to solve a two dimensional heat conduction problem using a set of empirical eigenfunctions, obtained from the Karhunen-Loève decomposition of the problem, in way to convert a given system into a model with the minimum degree of freedom.

One important application that involves the use of IHTPs is the experimental analysis of the re-entry phase which is of primary importance for the design of spacecrafts and for dimensioning the thermal protection system. Usually experiments are carried out in hypersonic wind tunnel to estimate heat flux considering all the phenomena that could be encountered during the re-entry flight. Particularly, on the control surfaces, where deflections are present, Görtler vortices could be induced by the boundary layer instability due to the concave curvature on a turned flap. These vortices are longitudinal, stationary, and counter rotating [26]. Their occurrence during the laminar and transitional phases of the flight may considerably modify the heat flux. Streamwise rolls give rise to longitudinal striations of high and low heat flux with a known spatial frequency. They can lead not only to local, but also to global enhancements of heat transfer up to 100% according to the literature [27] and are object of recent researches (a visualization of Görtler vortices was performed by Schülein et al. [28] on a compression ramp in hypersonic flow in which the flow was perturbed by a zig zag strip mounted on the leading edge of the model).

IR thermography is often used in hypersonic flow to obtain the temperature distribution because of the presence of high spatial gradient caused by vortical structures; for example, de Luca et al. [29,30] analysed some aspects of shock wave boundary layer interaction (SWBLI) in a two dimensional hypersonic wedge flow over a flat plate/ramp configuration where the effect of the tangential conduction, due to the formation of Görtler type vortices induce by a strip installed on the leading edge, are relevant. Also Schrijer [31] investigated the effect of Görtler on heat transfer on hypersonic flow on a double compression ramp using Cook & Felderman equation. Another type of application was made by dello Ioio [32] who studied the heat transfer in hypersonic flow on a double cone and showed a data reduction technique based on least squares error method.

In this work, a data reduction technique to solve 1-D and 2-D IHTPs is shown where temperature distribution on the surface of the model is measured by an IR camera. In paragraph 2 the topic of images restoration to avoid distortion effects [33] and oscillations caused by aerodynamic forces is discussed.. On the rebuilt images the inverse heat problem is solved in the 1-D [32] and 2-D cases using an approach based on the least square method. In the solution of the 2-D problem it is necessary to take into account the higher computational cost. Hence, a reduction method based on Fourier transform is shown. The methodology has been numerically validated as described in paragraph 3 and then applied to experimental tests carried out in the hypersonic wind tunnel of the University of Delft at a Mach number equal to 7.5. At least, in paragraph 5 a comparison between 1-D and 2-D solutions is made.

2 Data reduction

2.1 Image restoration

According to Cardone et al. [33] infrared data obtained by an infrared camera are available in form of 2-D images while the observed surfaces are often not planar. As a matter of fact, even when model surfaces are planar (e.g. a compression ramp) optical deformations must be taken into account.

To rebuilt the image a target with IR control points, as shown in figure 1, is applied on the surface under investigation and an IR image is acquired. In this way the transformation matrix between real coordinates of the markers and their coordinates in the image reference system is obtained [33] and it is used to reconstruct the surface of the 3-D model in way to obtain the correct temperature in each point of the rebuilt model. In a general approach also the effects of the directional emissivity must be considered to rebuild the IR images.

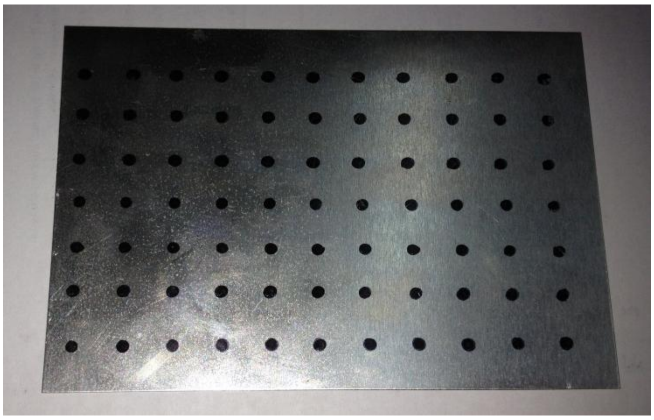

Fig. 1. Target used in the calibration procedure.

Images restoration is completed after removingmodel oscillations caused by aerodynamic forces from the infrared images. In this way, no errors are made during the reconstruction of the temperature rise in each point of the model surface. A simple technique based on geometrical observation is used detecting the corners points of the model. Since during the test the temperature on the leading edge of the model under investigation is higher than ambient temperature it is simple to identify leading edge corners with an accuracy of the pixel. Assuming that the model is a rigid body, it can be stated that for each IR image a rotation and translation can be applied based on the straight-line equation through the detected points. In this way the IR images are mapped on the correct coordinates and a new image is obtained. An example of image restoration is shown in figure 2 where a typical original IR image and a restored one are presented.

The last step necessary, before starting the solution of the IHTP, is to define the first and the last images of interest to build correctly the experimentally temperature rises in each point of the domain to be used for the IHTP, according to dello Ioio [32].

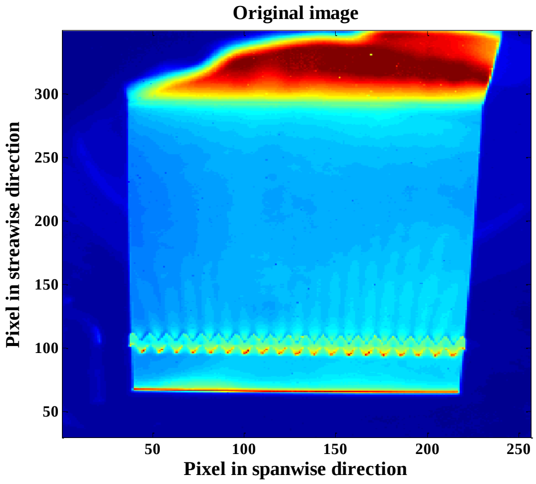

(a)

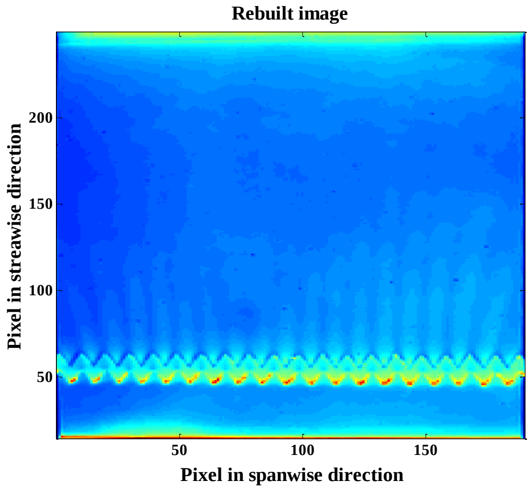

(b)

Fig. 2. (a) A visualization of the IR image before the calibration procedure;
(b)A visualization of the rebuilt image after the calibration procedure.

2.2 IHTP solution

To solve in this work the IHTP the heat equation inside the body, reported in eq. 1, has been solved firstly directly:

$$K\,\nabla^2(T) = \rho c_p \frac{\partial T}{\partial t} \tag{1}$$

with boundary conditions

$$\begin{cases} T(x,y,z,0) = T_{wi} \\ K\,\frac{\partial T(x,y,z,t)}{\partial n}\Big|_S = q_w(t)\ \ or\ \ T(x,y,z\ \in S,t) = T_S(t) \end{cases} \tag{2}$$

where K is the thermal conductivity, ρ is the density, c_p is the specific heat and T_{wi} is the initial temperature.

The initial temperature distribution T_{wi} is known and considered to be constant in all the domain. For the boundary condition at the far wall, any known temperature $T_S(t)$ or flux $q_w(t)$ can be used. In this work the wall *S* is considered as isotherm so that $T(x,y,z\ \in S,t) = T_S(t)$ but in a more realistic approach, the far wall can be considered adiabatic. This is true in most wind tunnels, in which the test chamber pressure is very low (of the order of the millibar), there is no flow on the far wall and the far wall itself is at significantly lower temperature than the surface exposed to the flux; in this situation, both convective and radiative heat fluxes are negligible and the far wall effectively behaves as an adiabatic wall.

The unknown heat flux $q_w(t)$ is defined in equation (3).

$$q_w(t) = h(T_w - T_{aw}) + \sigma\varepsilon(T_w^4 - T_r^4) \tag{3}$$

$q_w(t)$ depends on the convective heat transfer coefficient *h* which is unknown and needs to be estimated, the wall temperature T_w which is known from the numerical solution of the equation system, the adiabatic wall temperature T_{aw} which is not known exactly and can either be estimated either set to the known total temperature, ε which is the surface emissivity of the model and is known either from literature or from experimental calibration, σ which is the Stefan–Boltzmann constant and T_r is a reference temperature towards which the model radiates and in this work is considered to be the same as the ambient temperature. It is important to highlight that this model evaluates explicitly the radiative heat flux whose contribution can be important in tests in wind tunnels, where the surface temperatures can reach high values.

The approach used in this work is the least-square method and particularly, in this context, the only parameter which must be estimated is the convective heat transfer coefficient *h*, which is a function, generally, of both streamwise and spanwise coordinates. As a consequence, the optimization process consists in varying the parameter under optimization, *h*, on which the convective heat flux depends, in order to minimize the functional of the sum of the squared differences between the measured temperatures, $T_{w_{TH}}(t)$, and the temperatures $T_{w_{NUM}}(t)$ generated numerically by the direct solution of the equation system:

$$\int_0^{t_p} \left(T_{w_{TH}}(t) - T_{w_{NUM}}(t)\right)^2 dt \tag{4}$$

It is clear that the estimation of the heat flux relies on the estimation of the parameter *h*. The evolution of surface temperature on the tested body is measured with the help of IR thermography; for each point of the surface the experimental temperature rise $T_{w_{TH}}(t)$ is therefore known. $T_{w_{TH}}(t)$ is made up of a number *N* of temperature measurements which depends on the frequency of acquisition of the thermograph, f_s , and on the duration of test t_p . To estimate the heat flux it is necessary firstly to set all the known values (T_r,T_{wi}) and to set a trial value of the unknown parameter *h*. At each iteration the heat equation is solved and the parameter *h* is modified in attempt to minimize the error functional.

The optimization method used in this work is based on the solution of nonlinear least-square problems of the form:

$$\min_x \|f(x)\|_2^2 = \min_x (f_1(x)^2 + f_2(x)^2 + f_n(x)^2) \tag{5}$$

where *x* is a vector and *f(x)* is a function that returns a vector value. This algorithm chooses the trust-region-reflective algorithm to minimize this problem [34,35]. To understand the trust−region approach consider the unconstrained minimization problem, minimize *f(x)*, where the function takes vector arguments and returns scalars. Suppose to be at a point x in n−space and to want to improve, i.e., move to a point with a lower function value. The basic idea is to approximate *f* with a simpler function *q*, which reasonably reflects the behaviour of function *f* in a neighbourhood N around the point *x*. This neighbourhood is the trust region. A trial step *s* is computed by minimizing (or approximately minimizing) over N. This is the trust−region sub-problem

$$\min_s \{q(s),\ s \in N\} \tag{6}$$

The current point is updated to be *x + s* if *f(x+s)<f(x)*; otherwise, the current point remains unchanged and N, the region of trust, is shrunk and the trial step computation is repeated.

The choice and computation of the approximation *q* (defined at the current point *x*) and the choice of the trust region N are the main aspect in trust region optimization. In the standard trust−region method [36], the quadratic approximation *q* is defined by the first two terms of the Taylor approximation to *f* at *x*; the neighbourhood N is usually spherical or ellipsoidal in shape. Mathematically the trust−region sub-problem is typically stated

$$\min \quad \left\{\frac{1}{2} s^T H s + s^T g \ such\ that\ \|Ds\| \le \Delta\right\} \tag{7}$$

where *g* is the gradient of *f* at the current point *x*, *H* is the Hessian matrix (the symmetric matrix of second derivatives), *D* is a diagonal scaling matrix, Δ is a positive scalar, and ‖ ‖ is the 2−norm. Such algorithms provide an accurate solution to eq. 7. However, they require time proportional to several factorizations of H. Therefore, for large−scale problems a different approach is needed. Several approximations and heuristic strategies, based on eq. 7, have been proposed in the literature [37,38]. The approximation approach followed in the present algorithm is to restrict the trust−region sub-problem to a two−dimensional subspace S [39].

This data reduction technique has been applied to the 1-D case, in which the heat transfer problem has been solved using a parabolic partial differential equations solving algorithm [40,32], and also to the 2-D case, in which the heat transfer problem has been solved using a finite element code [41].

2.3 2-D inverse heat transfer problem

To solve a 2-D IHTP it is necessary to take into account that the number of parameters to estimate contemporaneously is higher than in the 1-D solution. As a matter of fact if *n* is the number of pixel in the spanwise direction, the function *h* is at least made up of *n* elements and for each line under investigation *n* parameters at the same time must be estimated; consequently, the computational cost related to the solution of the 2-D IHTP is higher than in the 1-D case.

The 2-D IHTP is solved reducing the computational cost representing the function *h* using a lower number of parameters; hence, the unknown function can be represented using the discrete Fourier transformed (DFT) and taking only a finite number of coefficients. According to De Luca and Cardone [42] the response of the picture elements of the IR image have to be considered as independent thus applying the Nyquist theorem the maximum measured spatial frequency of the heat transfer distribution is the frequency corresponding to a period of two picture elements.

The number of coefficients of the discrete Fourier transformed to be taken into account is indeed dependent on the shape of the function *h* and is lower with respect to this theoretical limit; to establish this number the solution obtained from the 1-D IHTP is used: doing a spectral analysis of the signal the maximum frequency to be taken into account is identified.

To transform the signal correctly using the DFT it must be periodic otherwise as observed by Astarita [43] the Gibbs phenomenon, linked to the discontinuity between the last and the first point of the input signal, may be present. To avoid this effect the input signal may be duplicated using a function to join the first and the last point in way that the function is continuous and with a continuous first derivative; a way to do it is to use a third order polynomial function which passes through the last two points and that at a chosen distance, in way that the signal is improved at least of 40% of the input one, also passes through the first two points of the input signal.

Once the function is extended and the minimum number of coefficient to represent the function *h* is chosen the 2-D IHTP may be solved considering that the input function can be represented using a number of coefficients *m* lower than *n* (it is not possible to define a priori the effective computational cost reduction because it depends on the shape of the function *h*). Thus, the vector *x* in eq. 5 is constituted by *m* elements. At the same time, the heat equation is solved directly considering that each line is constituted by *n* elements; to do this step it is necessary to use the inverse Fourier transform (IFT) of the transformed signal of *h*. In this way the problem is solved reducing the computational cost but at the same time there is no losses in the estimation of the numerical temperature rise.

3 Numerical validation

The proposed methodology is validated numerically to analyse the error made by the heat flux sensor in the estimation of *h*, as meaningful parameter characterizing each temperature rise, in order to identify its limits of applicability.

The validation method can be outlined as described below. For a given time of the test and a given heat flux distribution an "experimental" temperature rise is generated numerically solving the heat equation (eq.1 and eq.2); a random noise with a fixed mean value (β_{noise}) and known standard deviation (σ_{noise}) is added to the temperature rise generated at the step before to obtain the noisy temperature rise. This is the temperature rise that is given as an input to the optimization routine and the inverse heat transfer problem is solved. For a fixed bias and standard deviation of the noise, the validation is repeated several times in order to estimate errors.

For the present work two different periodical heat flux distributions characterized by two values of the spatial frequency have been assumed to analyse the effect of the spatial frequency on the accuracy of the estimation. For each case two different types of noise have been added: mean value and standard deviation of 0.4 K; mean value and standard deviation of 0.8 K. Although modern thermographs feature very low noise levels (for the CEDIP Titanium 530L the NETD is 25 mK at the ambient temperature) higher levels of noise are expected in wind tunnel experiments.

It is necessary to define a number of parameters capable to describe unequivocally the goodness of the optimization. If *p* is the exact value of the parameter to estimate, p_i the value of that parameter as estimated in the generic optimization *i* and

$$\overline{p} = \frac{1}{n}\sum_1^n p_i \tag{8}$$

the average value of the total number of estimations, we can define the following error parameters:

$$\beta = \overline{p} - p \tag{9}$$

$$\sigma = \sqrt{\frac{1}{n}\sum_1^n (p_i - \overline{p})^2} \tag{10}$$

where β is the bias that shows the difference between the exact value and its ideal estimation; σ is the standard deviation that is a measure of the oscillations around the average in the estimation under investigation.

In figure 3 and figure 4 are shown numerical validation results. Normalised bias and normalised standard deviation are plotted as a function of the test time (t_p) and the analysis is performed for several test time. The highest test time taken into consideration is equal to 0.2 s which is the test time of the Hypersonic Test Facility Delft (HTFD) in which expertimental tests, as discussed in the section below, has been carried out.

In figures 3a and 4a the normalized bias in the estimation of the convective heat transfer coefficient is shown while in figures 3b and 4b the normalized deviation standard in the estimation of the convective heat transfer is shown. As can be seen, both the bias and the standard deviation decrease increasing test time and it is possible to note that bias error made in the estimation is a function of the noise added and of the spatial frequency of the convective heat transfer coefficient. It is also clear that for the highest test times considered, the influence of the spatial wavelength of the signal is less relevant. In the worst case (σ_{noise}=0.8K, β_{noise}=0.8K) the bias error made is lower than 3% while the standard deviation error is lower than 0.3%. Considering the approximations made to reduce the computational cost and the complexity in optimizing vectors of high dimensions errors made compared with dello Ioio [32] are acceptable. Also the shape of curves represented in figures 3 and 4 are comparable with dello Ioio [32].

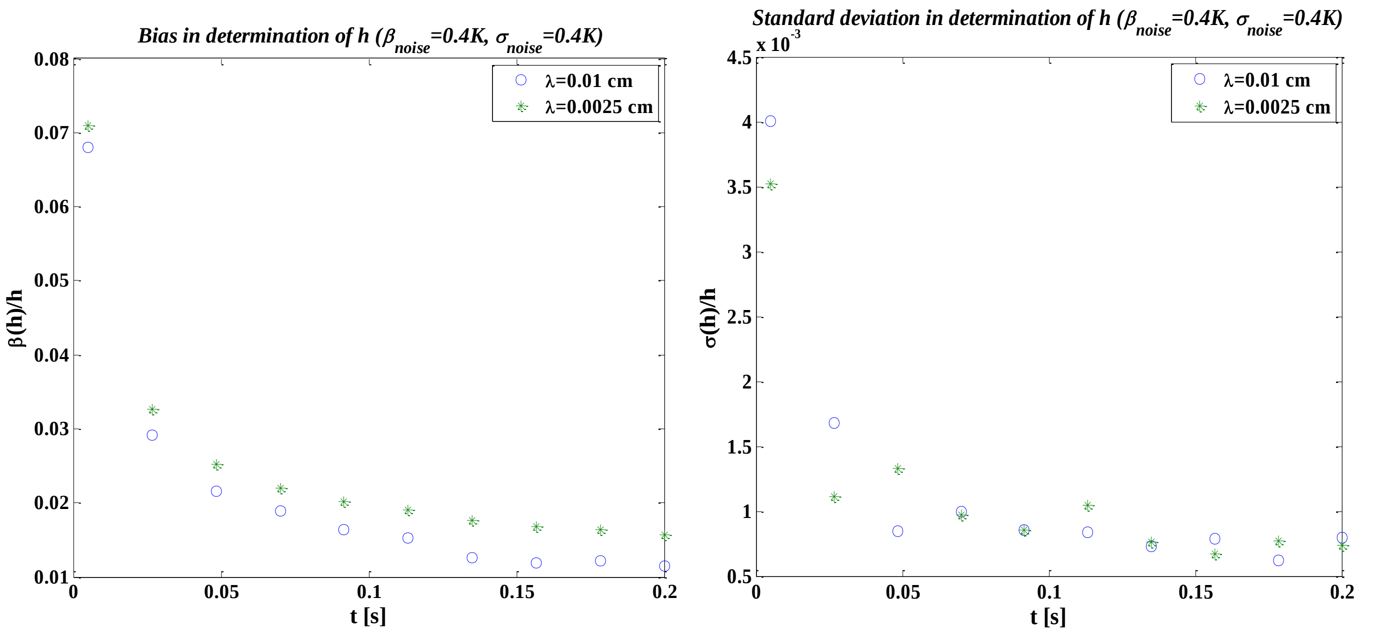

(a) (b)

Fig.3. (a)Bias 2-D solution for β_{noise}=0.4K and σ_{noise}=0.4K for λ=0.01 cm and λ=0.0025 cm;
(b) Standard deviation for β_{noise}=0.4K and σ_{noise}=0.4K for λ=0.01 cm and λ=0.0025 cm.

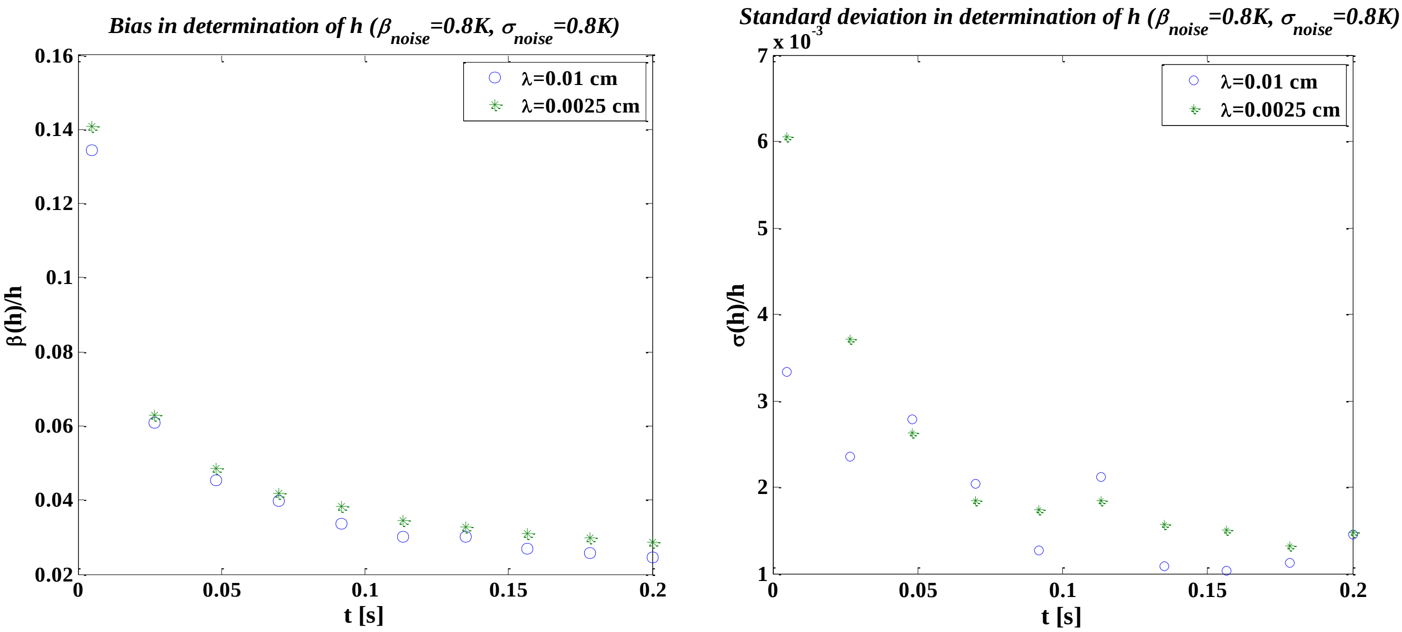

(a) (b)

Fig.4. (a)Bias 2-D solution for β_{noise}=0.8K and σ_{noise}=0.8K for λ=0.01 cm and λ=0.0025 cm;
(b) Standard deviation for β_{noise}=0.8K and σ_{noise}=0.8K for λ=0.01 cm and λ=0.0025 cm.

4 Experimental apparatus

The Hypersonic Test Facility Delft (HTFD) is a Ludwieg tube concept tunnel. This concept relies on the principle of a high pressure difference between the storage tube and the vacuum charge tank with a fact acting valve upstream of the nozzle. When the fast acting valve is opened, an expansion wave travels into the storage tube and accelerates the flow from the high pressure tube into the vacuum charge tank. The running time of the HTFD is approximately 100 ms which is defined as the time it takes for the particle at the most upstream location of the storage tube to reach the valve. This particle path is indicated in the (x,t) diagram given in figure 5a by DCE. This can be determined based on simple wave theory and thus it is dependent on the length of the storage tube, the initial speed of sound and the Mach number downstream of the expansion wave that travels into the storage tube [43].

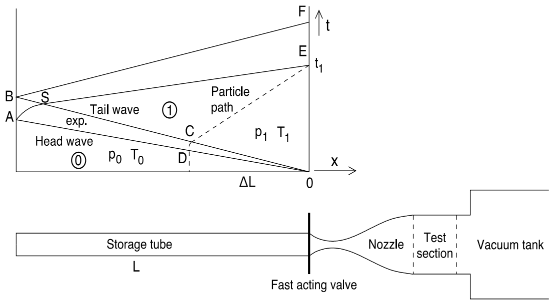

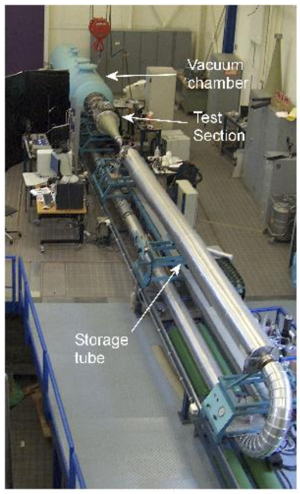

(a) (b)

Fig.5. (a) Operational principle of the Ludwieg tube;
(b) The Hypersonic Test Facility Delft.

The storage tube is heated to prevent condensation. A tandem nozzle is used to set the appropriate flow conditions. The pressure in the storage tube can be varied and the free stream pressure is then calculated based on the geometrical relations of the tandem nozzle. For the test cases discussed here, the following flow properties are set.

$T_t\,[K]$	$T\,[K]$	$p_t\,[bar]$	$U\,[m/s]$	$Re/m\,[m^{-1}]$
579	47	28	1033	11.05 x 10^6

Table 1. Flow properties for the test case analysed in this work.

The Infrared measurements are performed on a double compression ramp wind tunnel model, which is made of Makrolon. Makrolon has a conductivity of $k = 0.20\,W/Km$ and as a result a high surface emissivity is measured ($\epsilon = 0.88$) [45]. Next to that, this polycarbonate material can withstand temperatures of $120C°$ without changing the material properties. During the experimental campaign the model was painted black and the viewing angle with respect to the surface normal was less than 50 degrees in order to avoid the effect of the directional emissivity [46].

The first ramp has a length of 149 mm and an makes an angle with respect to the longitudinal wind tunnel axis of 5°. The second ramp is 57 mm in stream wise direction and makes an angle of 45°. A drawing of the model is given in figure 6a.

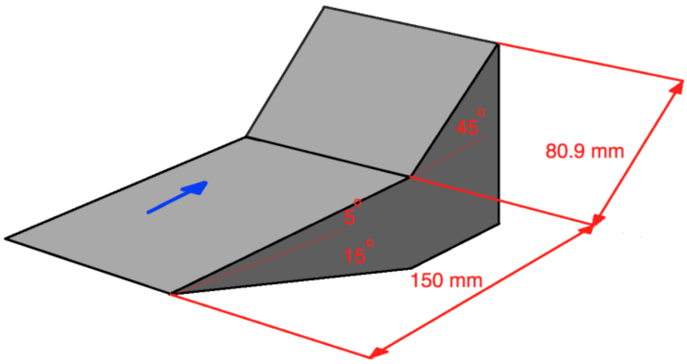

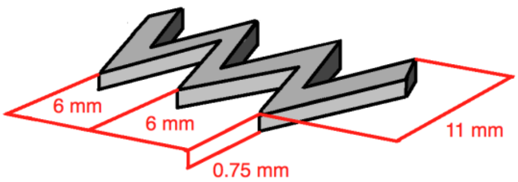

(a) (b)

Fig. 6. (a) A sketch of the model used during the experimental tests;
(b) A sketch of the comb-like strip puts on the model.

The comb-like strip which induces the longitudinal vortices is shown in figure 6b. The spanwise centre line of the comb-like strip is placed at 2.5 cm from the leading edge of the model.

The QIRT measurements are performed using the CEDIP Titanium 530L measurement system. The camera has a Mercury Cadmium Telluride (MCT) quantum detector array of 320 by 256 pixels and a spectral response of 7.7-9.3 μm. The camera has a maximum frame rate of 250 Hz at full resolution. During the measurements the integration time of the camera was set to either 17 or 340 μs depending on the expected temperature range. The model should be optical accessible and therefore a window of Germanium is used which has a transmissivity of approximately 0.8.

The camera is set – up under an angle with respect to the germanium window to prevent self reflection. Next to that, the camera and the window are covered by sheets to prevent reflections from the background. A sketch of the camera set-up is given in figure 7.

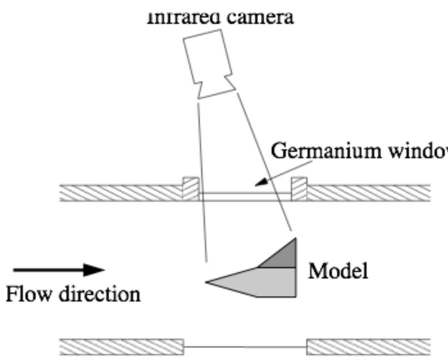

Fig. 7. A sketch of the camera set-up.

The response of a pixel in the IR camera can be approximated by a linear function defined by its gain $\alpha_{i,j}$ and a offset $\beta_{i,j}$ defined in equation 11

$$Y_{i,j} = \alpha_{i,j} X_{i,j} + \beta_{i,j} \tag{11}$$

This linear function should be equal for every individual pixel present in the sensor. To achieve this, a black body is presented to the sensor at two different exposure times and the average linear function is determined. This is followed by setting all the response functions equal to this average linear function such that every pixel response in the same way for every exposure time.

The CEDIP camera is fitted with a matrix detector which consists of a set of pixels. It can occur that some of these small detectors. They detectors are build up of a photosensitive plate and read circuit with in between Indium balls which are approximately 15 to 30μm. The size of the elements and the procedures carried out by the connections between the elements induce defects which affect a few elements. These are called bad pixels where the noise part of the signal is dominating. The software accompanied with the camera solves this problem by looking at the surrounding elements of the bad pixel. The algorithm tests up to 48 neighbouring pixels and replaces the bad pixel with the value of a neighbouring pixel.

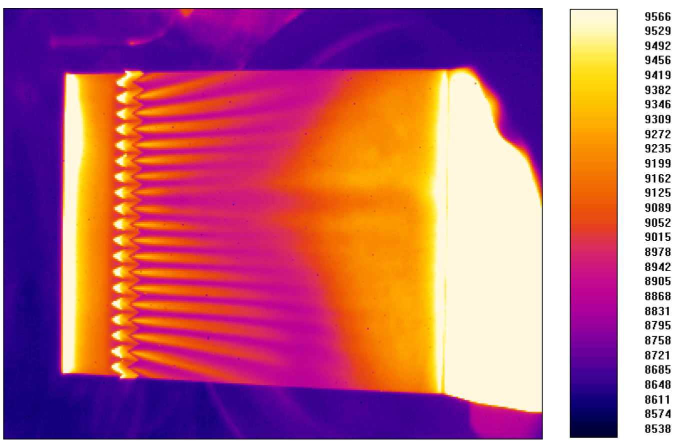

Fig. 8. IR image obtained during the experimental test (colour-bar in IU).

5 Experimental test

The methodology described before to solve 1-D and 2-D IHTPs is then applied on an experimental test carried out in the HTFD as reported in paragraph 4.In figure 8 is shown an IR image of the flow on the double compression ramp. As can be seen, the comb-like strip puts on the leading edge of the first ramp generates flow instability in form of vortices with spatial frequency equal to the distance between the teeth. In the image it is possible to see the separation region that is not symmetric. This phenomena is related to the comb like strip that is not perfectly pasted on the leading edge. As a consequence also the convective heat transfer coefficient distribution is characterized by a similar shape as shown in figure 9. The similarity in the shape is due to the hypothesis made in expression of the heat flux used in the direct solution of the heat equation. In figure 8 it is possible to note that on the second ramp temperature is higher and it difficult

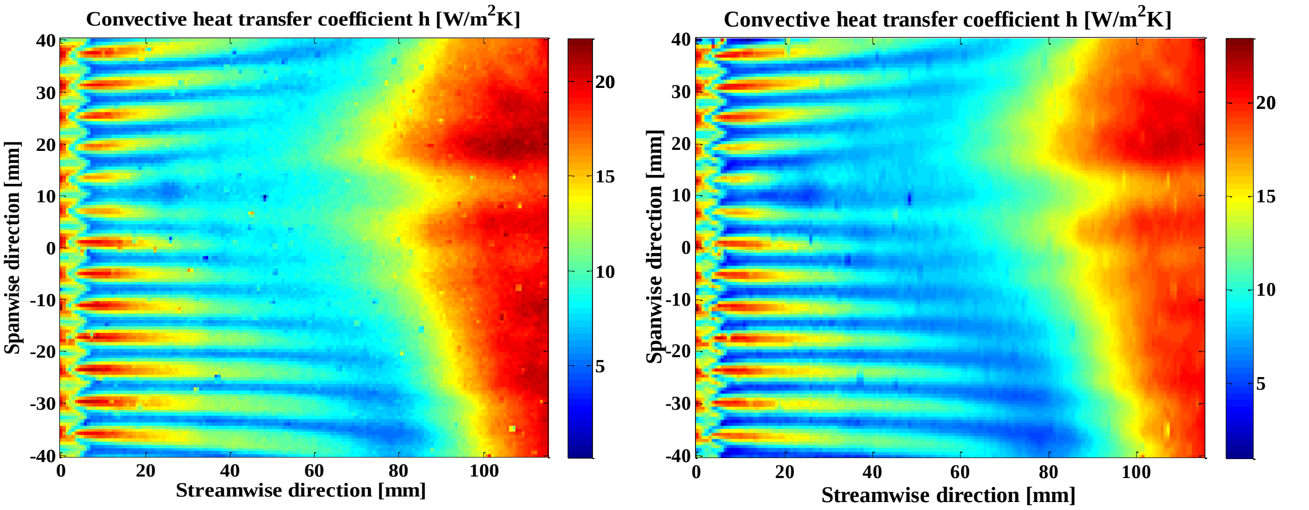

(a) (b)

Fig. 9 (a) Heat transfer coefficient distribution obtained from 1D solution;
(b) Heat transfer coefficient distribution obtained from 2D solution.

detect it using the same integration time used to record first ramp IR images. Furthermore, spanwise oscillations are clearly visible near the strip but further downstream the effect decreases. This is due to the increase in boundary layer thickness when moving downstream and the fact that the fact that the vortices are mainly located in the upper part of the boundary layer.

In figures 9a and 9b convective heat transfer coefficient distribution, starting from the comb-like strip, obtained using the 1-D and 2-D codes are shown. Analysing these figures it is possible note that using DFT to reproduce the forcing term of the equation the effect of the noise are lower than in the 2-D solution and it is also evident that the 2-D solution permits a more accurate solution of the problem. As a matter of fact along the line at 60 mm from the leading edge in the 2-D solution the vertical structures are present while in the 1-D solution they are not visible. In both cases the separation region, represented by the highest convective heat flux coefficient, is easily to pick out.

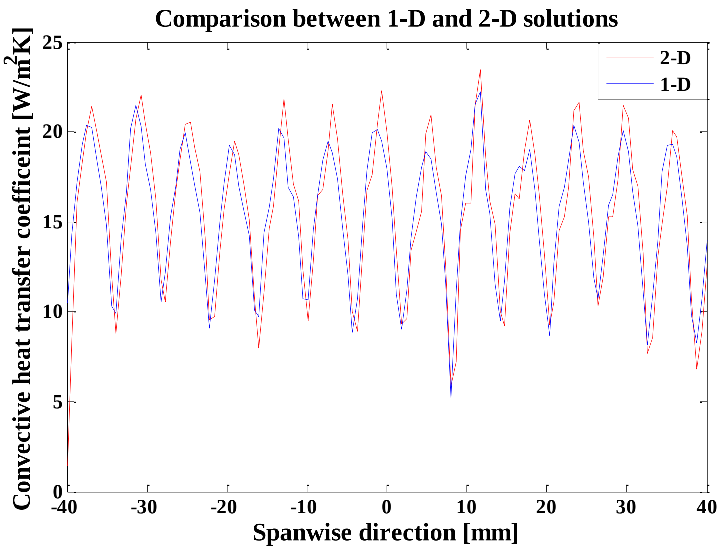

Fig. 10 A comparison between the 1D solution and 2D solution.

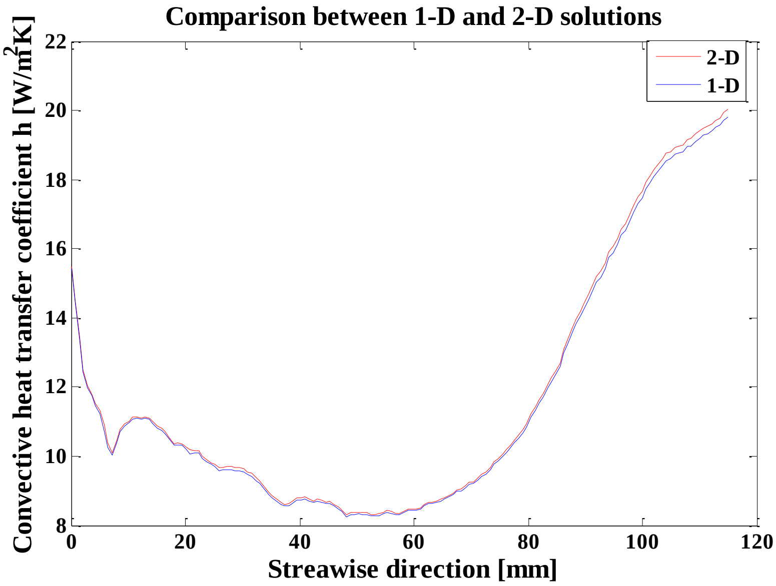

Fig. 11. A comparison between 1-D and 2-D solution in streamwise direction

In figure 10 there is a comparison, between the solution obtained applying the two codes. Note that in the 2-D solution the relative extrema are higher than for 1-D solution but the mean value is the same; this difference is related to the tangential conduction that cannot be evaluated using a 1-D code. The maximum difference between the peaks is about 20%. As reported in figure 10 the 1-D solution is similar to the 2-D and this result corresponds to what was found by Carlomagno and Cardone [13] in which the effect of tangential conduction is analysed as a function of a modified Fourier number; the periodical shape of the convective heat flux coefficient distribution along each line in spanwise direction are similar to the one reported by Schrjier [47]. In figure 11 there is also a comparison of the convective heat flux distribution mediated in the spanwise direction. It is evident that 1-D and 2-D solutions are more similar than in the streamwise direction as a consequence of the higher tangential conduction related to the vortices in the spanwise direction than in streawise one. The separation at about x=50 mm is visible.

6 Conclusion

In this work a data reduction technique to solve two dimensional inverse heat transfer problems for the evaluation of heat transfer by IR thermography measurements has been developed. In this work a pre-processing of IR images is made to remove distortion effect related to the representation of a three dimensional model on a two dimensional images and to eliminate vibrations due to the aerodynamic forces. The approach to solve inverse problems reduces the computational cost representing the heat flux by Fourier series and rebuilding taking into account only a finite number of frequencies.

The method has been numerically validated to evaluate limits of applicability of the approach proposed. From the analysis of the validation's results it is evident that errors made for time test of interest are acceptable and that the standard deviation in the estimation of the estimated parameter h is negligible as a consequence of Fourier discretization.

The approach has been applied to an experimental test carried out in a hypersonic wind tunnel. A comparison between the 2-D solution and a 1-D solution has been done and results show that the former presents a higher accuracy of the solution and gives the opportunity to visualize vortices which are not evident in the second case. At least a comparison of the convective heat transfer coefficient distribution in the spanwise direction has been done and the effect of the tangential conduction are evaluable considering that peaks are higher in the 2-D solution

7 References

[1]Giordano R., Ianiro A., Astarita T., Carlomagno G.M., 2011. Flow field and heat transfer on the base surface of a finite circular cylinder in crossflow. *Applied Thermal Engineering*, 1-10.

[2]De Luca L., Guglieri G., Cardone G., Carlomagno G.M., 1996. Experimental analysis of surface flow on a delta wing by infrared thermography. *AIAA Journal on Disc 1*.

[3]T. Astarita, Cardone G., Carlomagno G.M., 2006. Infrared thermography: An Optical method in heat transfer and fluid flow visualization, *Optics and Lasers Engineering 44*, 261-281.

[4]Walker D.G., Scott E.P., 1998. Evaluation of Estimation Methods for High Unsteady Heat Fluxes from Surface Measurements. *Journal of Thermophysics and Heat Transfer*, 12: 543-551.

[5]J.V. Beck, B. Blackwell, C. St. Clair Jr., 1985. Inverse Heat Conduction: Ill-posed Problems, Wiley Interscience.

[6]Cook W.J., Felderman E.J., 1966. Reduction of data from thin film heat transfer gauges: a concise numerical technique, *AIAA Journal 4*, 561-562

[7]C.C. Ji, P.-C. Tuan, H.-Y. Jang, 1997. A recursive least-squares algorithm for on-line 1-D inverse heat conduction estimation, *Int. J. Heat Mass Transfer 40,* 2081-2096.

[8]F. Scarpa, G. Milano, 1995. Kalman smoothing technique applied to the inverse heat conduction problem, *Numer. Heat Transfer 28*, 79-96.

[9]M. Raynaud, J.V. Beck, 1988. Methodology for comparison of inverse heat conduction methods, *J. Heat Transfer 110*,30-37.

[10]Raynaud M. , Bransier J., 1986. A new finite-difference method for the non-linear inverse heat conduction problem, *Numerical Heat Transfer,* 27-42.

[11]Shenefelt J.R., Luck R., Taylor R.P., Berry J.T, 2002. Solution to inverse heat conduction problems employing singular value decomposition and model-reduction, *International Journal of Heat and Mass Transfer 45*, 67-74.

[12]F.F.J. Schrijer, 2012. Unsteady data reduction techniques for QIRT: consideration of temporal and spatial resolution, QIRT Conference 2012.

[13]Carlomagno G.M., Cardone G., 2010. Infrared thermography for convective heat transfer measurements, *Experiments in Fluids 49*, 1187-1218.

[14]AL-Najemi N. M., Osman A. M., El-Refaee M., Khnafer K.M., 1998. Two dimensional steady-state inverse heat conduction problems, *Int. Comm. Heat Mass Transfer 25*, 541-550.

[15]Chen H.T., Wu X.Y., 2008. Investigation of heat transfer coefficient in two- dimensional transient inverse heat conduction problems using the hybrid inverse scheme, *Int. J.Numer. Meth.Engng*, 107-122.

[16]P.-C. Tuan, C.C. Ji, L.-W. Fong, W.-T. Huang, 1996. An input estimation approach to on-line two-dimensional inverse heat conduction problems, *Numer. Heat Transfer B 29,* 345-363.

[17]A.M. Osman, K.J. Dowding, J.V. Beck, 1997. Numerical solution of the general two-dimensional inverse heat conduction problem, *ASME J. Heat Transfer 119*, 38-45

[18]Yang Ching-Yu, 1998. Solving the two dimensional inverse heat source problem through the linear least-sqares error method, *International Journal of Heat and Mass transfer 41*, 393-398.

[19]D. Petit, V. Debray, C. Le Niliot, R. Pasquetti, 1992. Identification of local heat transfer coefficient using a boundary formulation. *Comput. Meth. Heat Transfer*.

[20]F.F.J. Schrijer, D. Modenini 2009. Inverse Heat Transfer Measurements in a Supersonic Wind tunnel: Application to a Backward Facing Step. Proceedings of the 10th International Workshop on Advanced Infrared Technology and Applications.

[21]C.-H. Huang, C.-W. Chen, 1998. A boundary-element-based inverse problem of estimating boundary conditions in an irregular domain with statistical analysis, *Numer. Heat Transfer B 33*, 251-268.

[22]Yoshimura T., Ikuta K., 1985. Inverse Heat-Conduction Problem by Finite-Element Formulation, *Int. J. Syst. Sci.*, 32, 1365-1376.

[23]Hsu T., Sun N., Chen G., Gong Z., 1992. Finite Element Formulation for Two-Dimensional Heat Conduction Analysis, *ASME J. Heat Transfer,* 114, 553-557.

[24]Videcoq E., Petit D., 2001. Model reduction for the resolution of multidimensional inverse heat conduction, *International Journal of Heat and Mass Transfer 44*, 1899-1911.

[25]Park H.M., Chung O.Y., Lee J.H.,1999. On the solution of inverse heat transfer problem using the Karhunen-Loève Galerkin method, *International Journal of Heat and Mass Transfer 42*, 127-142.

[26]Saric, W. S., 1994. Görtler vortices. *Annu. Rev. Fluid Mech. 26*, 379-409.

[27]McCormack, P. D., Welker, H., and Kellher, M., 1990. Taylor-Görtler Vortices and Their effect on Heat Transfer. *J. Heat Transfer 92***,** 110-112.

[28]E. Schülein, V.M. Trofimov, 2010. Steady longitudinal vortices in supersonic turbulent separated flows, *Journal of Fluid Mechanics*, 1-26.

[29]de Luca L., Cardone G., Aymer de la Chavalerie D., 1993. Goertler instability of a hypersonic boundary layer. *Experiments in Fluids 16,*10-16.

[30]de Luca L., Cardone G., Aymer de la Chavalerie D. et al., 1995. Viscous interaction phenomena in hypersonic wedge flow, *AIAA J. 33*, 2293-2298.

[31]Schrijer F.F.J., 2010. Experimental investigation of re-entry aerodynamic phenomena, *Phd Thesis,* TU Delft.

[32]dello Ioio, 2008. An improved data reduction technique for heat transfer measurements in hypersonic flows, *PhD Thesis,* University of Naples.

[33]Cardone G., Ianiro A., dello Ioio G., Passaro A., 2012. Temperature maps measurements on 3D surfaces with infrared thermography, *Exp. Fluids 52*, 375-385.

[34]Coleman, T.F. and Y. Li, An Interior, 1996. Trust Region Approach for Nonlinear Minimization Subject to Bounds, *SIAM Journal on Optimization,* 6:418–445.

[35]Coleman, T.F. and Y. Li, 1994. On the Convergence of Reflective Newton Methods for Large-Scale Nonlinear Minimization Subject to Bounds, *Mathematical Programming,* 67:189-224.

[36]Moré, J.J. and D.C. Sorensen, 1983. Computing a Trust Region Step, *SIAM Journal on Scientific and Statistical Computing,* 3:553-572.

[37]Byrd, R.H., R.B. Schnabel, and G.A. Shultz, 1988.Approximate Solution of the Trust Region Problem by Minimization over Two-Dimensional Subspaces, *Mathematical Programming,* 40:247-263.

[38]Steihaug, T., 1983. The Conjugate Gradient Method and Trust Regions in Large Scale Optimization, *SIAM Journal on Numerical Analysis,* 20:626-637.
[39]Branch, M.A., T.F. Coleman, and Y. Li, 1999. A Subspace, Interior, and Conjugate Gradient Method for Large-Scale Bound-Constrained Minimization Problems, *SIAM Journal on Scientific* Computing, 21:1-23.
[40]Skeel, R. D. and M. Berzins, 1990. A Method for the Spatial Discretization of Parabolic Equations in One Space Variable, *SIAM Journal on Scientific and Statistical Computing,* 11:1–32.
[41]J. Alberty, C. Carstensen, S. A. Funken, 1999. Remarks around 50 lines of Matlab: Short finite element method implementation, *Numerical Algorithms*, 20:117-137.
[42]de Luca L., Cardone G., 1991. Modulation transfer function cascade model for a sampled IR imaging system, *Applied Optics*, 30: 1659-1664.
[43]Astarita T., 2008. Analysis of velocity interpolation schemes for image deformation methods in PIV. *Exp.Fluids,* 257-266.
[44]F.F.J. Schrijier, Bannink W.J., 2008. Description and Flow Assessment of the Delft Hypersonic Ludwieg Tube, 26th AIAA Aerodynamic Measurement Technology and Ground Testing Conference.
[45]F.F.J. Schrijier, F. Scarano, B.W. van Oudheusden, 2003. Transient heat transfer measurements on a blunted cone-flare model in a short duration hypersonic facility using quantitative infrared thermography, *7th Triennial International Symposium on Fluid Control, Measurement and Visualization.*
[46]Ianiro A., Cardone G., 2010. Measurements of surface temperature and emissivity with stereo dual-wavelength IR thermography. *Journal of Modern Optics 57*, 1708-1715.
[47]Schrjier F.F.J., 2010. Investigation of Görtler vortices in a hypersonic double compression ramp flow by means of infrared thermography. QIRT Conference 2010.